Electronic Supplementary Material (ESI) for Soft Matter.

Using Solution State NMR Spectroscopy to Probe NMR Invisible Gelators

Matthew Wallace,[a,*] Jonathan A. Iggo[a] and Dave J. Adams[a,*]

[a] *Department of Chemistry, University of Liverpool, Crown Street, Liverpool, L69 7ZD, U.K. Email: d.j.adams@liverpool.ac.uk*

Electronic Supplementary Information (ESI)

1. Calibration of method for *in situ* pH determination by NMR spectroscopy and discussion of errors

The limiting chemical shifts, δ_H and δ_L, of the indicators were determined by adjusting the pH of a H_2O solution of the indicators, held at 25°C in a thermostatic water bath, with NaOH/HCl and then measuring the ^{1}H NMR spectra of the solutions. A Hanna Instruments HI8424 pH meter equipped with an FC200 probe was used in these experiments. 32 pH values were tested, spanning the pH range 1-12. The performance of the indicators was found to be independent of the presence or absence of 50 mM NaCl (Figure S1a). The titration curves from these experiments were then fitted to Equation 6 with the error in δ taken as the standard fitting error, $\Delta\delta$, given by Equation 7 of Brown.[1] Data for glycine and methylphosphonic acid, both with two titratable groups, were fitted to Equation 4 of Szakács et al.[2] The fitted pK_as of all indicators were in agreement with the literature values given in the main text within the error of our pH meter of ca. ±0.2 units. These literature values were used in the calculation of the pH. When calculating a pH from chemical shifts, all indicators whose chemical shift lay within $\Delta\delta$ of their limiting values were excluded from the calculation. Errors in the calculated pH, ΔpH, were calculated using the equation:

$$\Delta pH = \frac{\Delta\delta(\delta_L - \delta_H)}{(\delta_L - \delta)(\delta - \delta_H)\ln(10)} \qquad \text{(S1)}$$

with the overall error calculated as an average of both indicators in the pair, weighted by their relative sensitivities. This error, which is displayed as error bars in Figures 4b and S1b, can be considered as a 'random' error. Between pH 6 and 3.5, this error is less than 0.1 units. Limiting chemical shifts of the indicators are provided in Table S1a.

Indicator	pK_a (fit)	pK_a (literature[3])	δ_H/ppm	δ_L/ppm	$\Delta\delta/10^{-3}$ ppm
Formic acid	3.54	3.75	8.241	8.454	1.89
Acetic acid	4.58	4.76	2.096	1.919	0.55
Methylphosphonic acid[4]	7.74 (2.17)	7.74 (2.38)	1.294	1.086	6.16
Glycine	9.91 (2.24)	9.78 (2.35)	3.563	3.186	2.62

Table S1a. Limiting chemical shifts of indicator compounds used in the study with sodium methanesulfonate (2.815 ppm) as a reference. Literature pK_a values were obtained from Reference 3 unless otherwise stated. The other pK_a values of glycine and methylphosphonic acid, not used in the pH calculation, are indicated in parentheses.

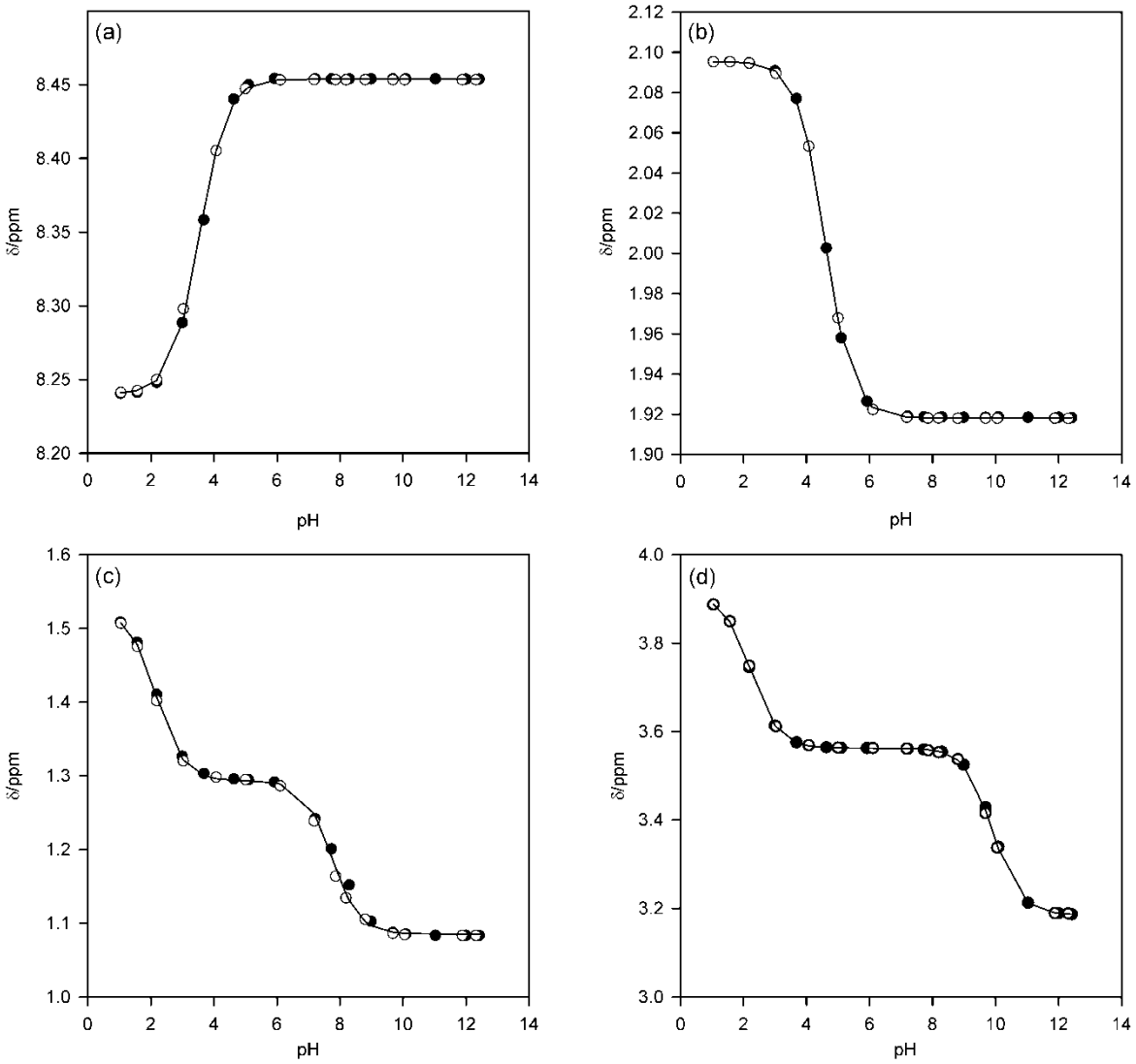

Figure S1a. Titration curves of indicators with (white circle) and without (black circle) 50 mM NaCl. Fits to the combined datasets are shown as solid lines. Formic acid (a), Acetic acid (b), Methylphosphonic acid (c) and Glycine (d).

The systematic error in the pH calculated using our method was assessed by determining the pK_as of a set of compounds using 'NMR titration' methods in which the chemical shifts of these molecules measured at different pH values, as determined by our NMR method, were fitted to Equation 6 to obtain a value for their pK_a. The compounds chosen for this part of study were l-alanine, 3-cyanophenol, imidazole, pyridine and glycolic acid. To generate 'NMR titration' data for these compounds, a solution of the compounds under study and the NMR pH indicators was prepared at pH 12 and the pH systematically lowered as the chemical shifts were recorded. For pyridine and glycolic acid, the pH was decreased *via* the slow hydrolysis in solution of glucono-δ-lactone (GdL). For imidazole, 3-cyanophenol and l-alanine the solution at high pH was carefully layered on top of solid GdL in the bottom of a 5 mm NMR tube to generate a vertical pH gradient across the sample which was imaged using chemical shift imaging (CSI) to obtain pH values and chemical shifts along

the length of the sample. For this purpose, a modified version of the gradient phase encoding sequence of Trigo-Mouriño et al.[5] - (π/2 - τ_1 - g - τ_2 - acquire, where g is a gradient pulse in the form of a smoothed square and τ_1 and τ_2 are delays of length 10 μs and 200 μs respectively) - was used with a double echo WATERGATE sequence of Liu et al.[6] (Bruker pulse program library ZGGPW5) in place of the π/2 pulse and a spoil pulse (1 ms, 27 G/cm) at the end of the signal acquisition period (1 s) to dephase any transverse magnetisation remaining before the next transient was acquired. 128 gradient increments from -27 to 27 G/cm with a gradient pulse duration of 238 μs were executed, each with 16 transients, affording a theoretical spatial resolution of 200 μm and a total acquisition time of 40 minutes. Additional data points for l-alanine at high pH were obtained *via* the slow hydrolysis in solution of sodium succinate mono-methyl ester. pK_as for the compounds under study determined using the 'NMR titration' method are given in Table S1b along with literature values. Titration curves are presented on Figure S1b with the error bars displaying ± the 'random' error in the pH. The measured pK_a values agree with the literature values within ±0.2 units while all fitted curves fit, in general, within the error bars. The error bars, calculated using Equation S1, are thus a reasonable estimate of the random error in a pH measurement while the measured values are systematically different from the true pH by less than 0.2 units.

Compound	pK_a ('NMR titration')	pK_a (literature[3])
Glycolic acid	3.86	3.83
Pyridine	5.36	5.23
Imidazole	6.98	6.99
3-cyanophenol	8.53	8.61
l-Alanine	9.93	9.87

Table S1b. pK_a values of compounds determined *via* the 'NMR titration' method and literature values from source indicated.

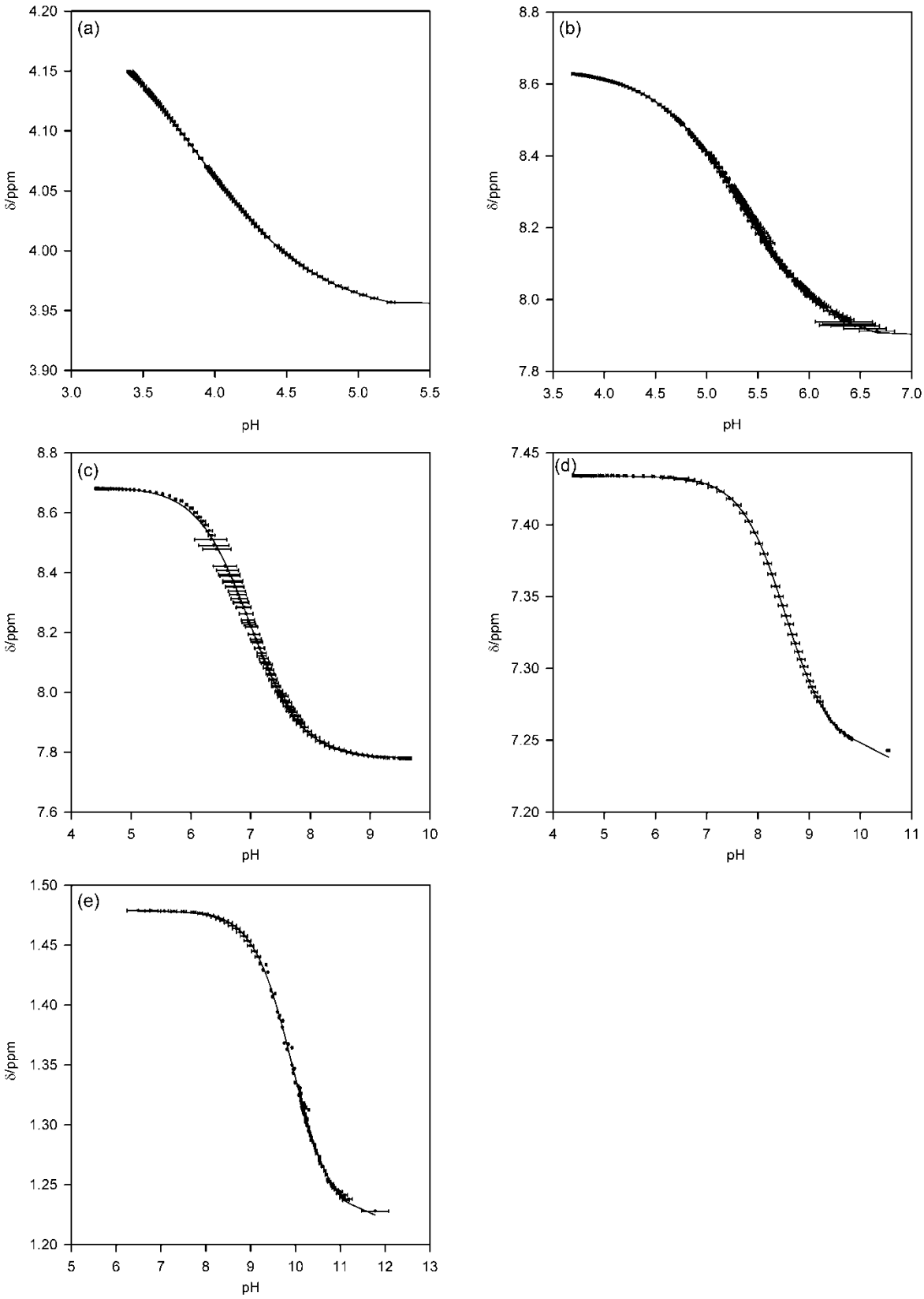

Figure S1b. NMR titration curves to determine pK_as of glycolic acid (a), pyridine (b), imidazole (c), 3-cyanophenol (d) and l-alanine (e). Error bars indicate the 'random' error in the pH, estimated from Equation S1. The scatter in the data for l-alanine around the centre of the titration curve is due to the broadness of the glycine resonance on the CSI spectra at these pH values.

2. Efficacy of ^{23}Na residual quadrupolar couplings to follow hydrogel development

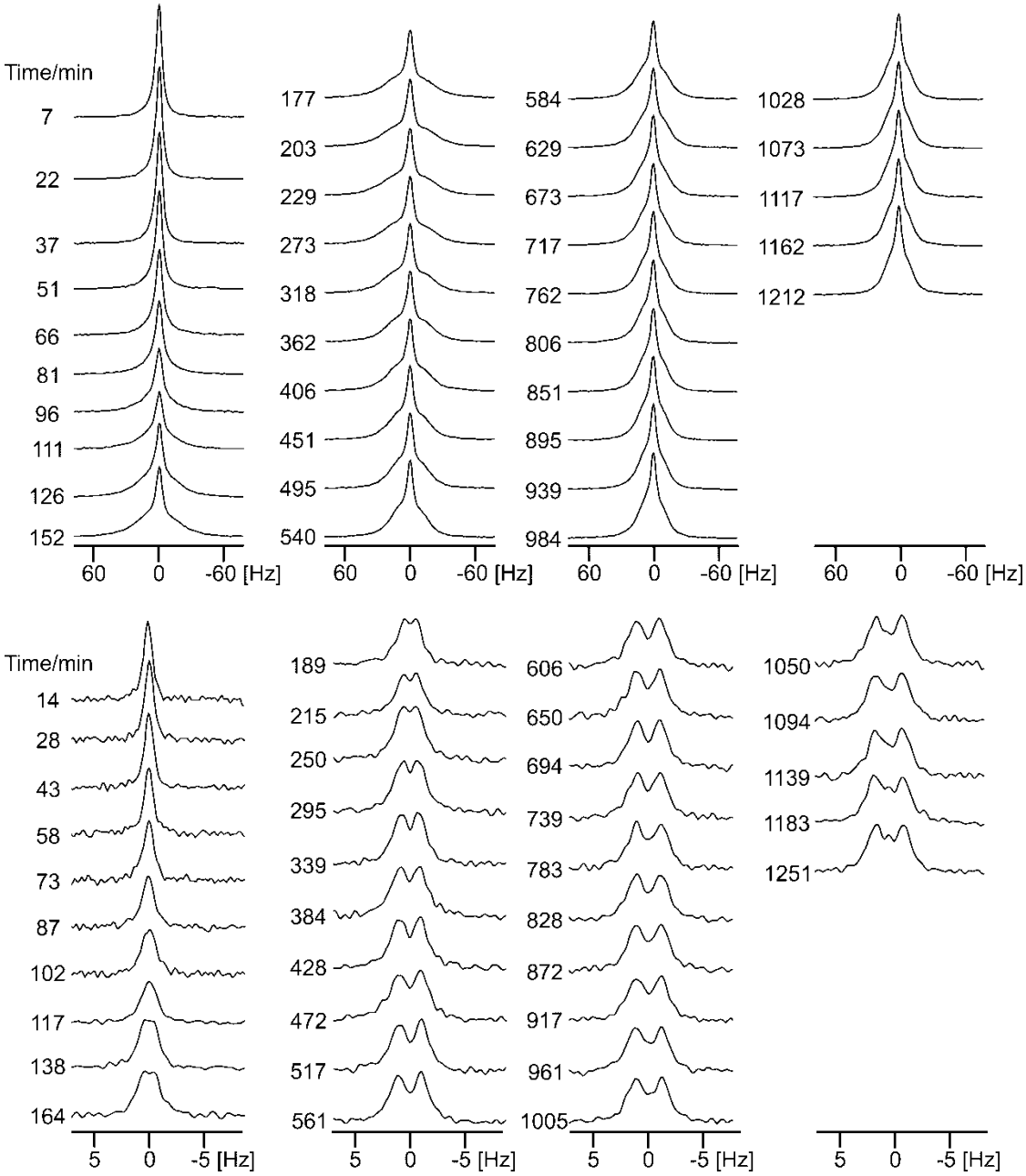

Figure S2. ^{23}Na (upper plots) and ^{2}H (IPA) NMR spectra (lower plots) at times indicated since the addition of GdL to a solution of **1** at high pH.

The sample was prepared according to the standard method described in the main text but without the addition of NH_4Cl. The ^{23}Na resonance exhibits a residual quadrupolar coupling which, like that of $^{14}NH_4^+$, is largest at ca. 150-200 minutes but gradually decreases as charge is lost from the gel fibres. Owing to ^{23}Na having a nuclear spin of 3/2 and quite broad lines, the RQC is apparent only as a broad feature on the base of the central -1/2↔1/2 transition and so cannot be reliably extracted. ^{23}Na spectra were recorded with 256 transients before and 512 transients after 120 minutes had elapsed, with 6144 points and a sweep width of 100 ppm, giving acquisition times of 1 minute 30 seconds and 3 minutes respectively.

3. Example ^{23}Na CPMG echo decays (T_2 measurement)

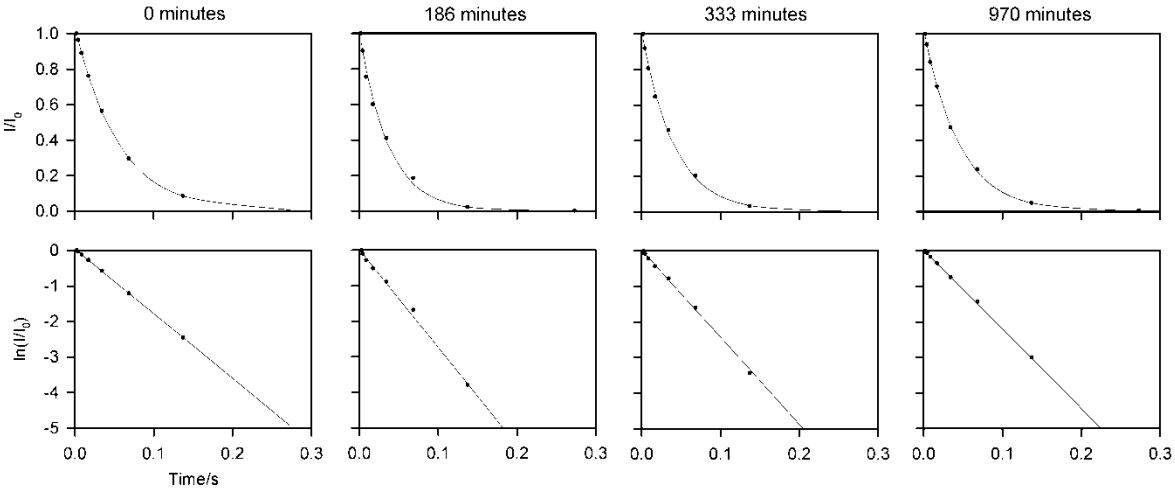

Figure S3. Example ^{23}Na CPMG echo decay plots, from data presented on Figure 1c, at times indicated since the addition of GdL.

4. Effect of added NMR probe molecules on the gelation process of **1**

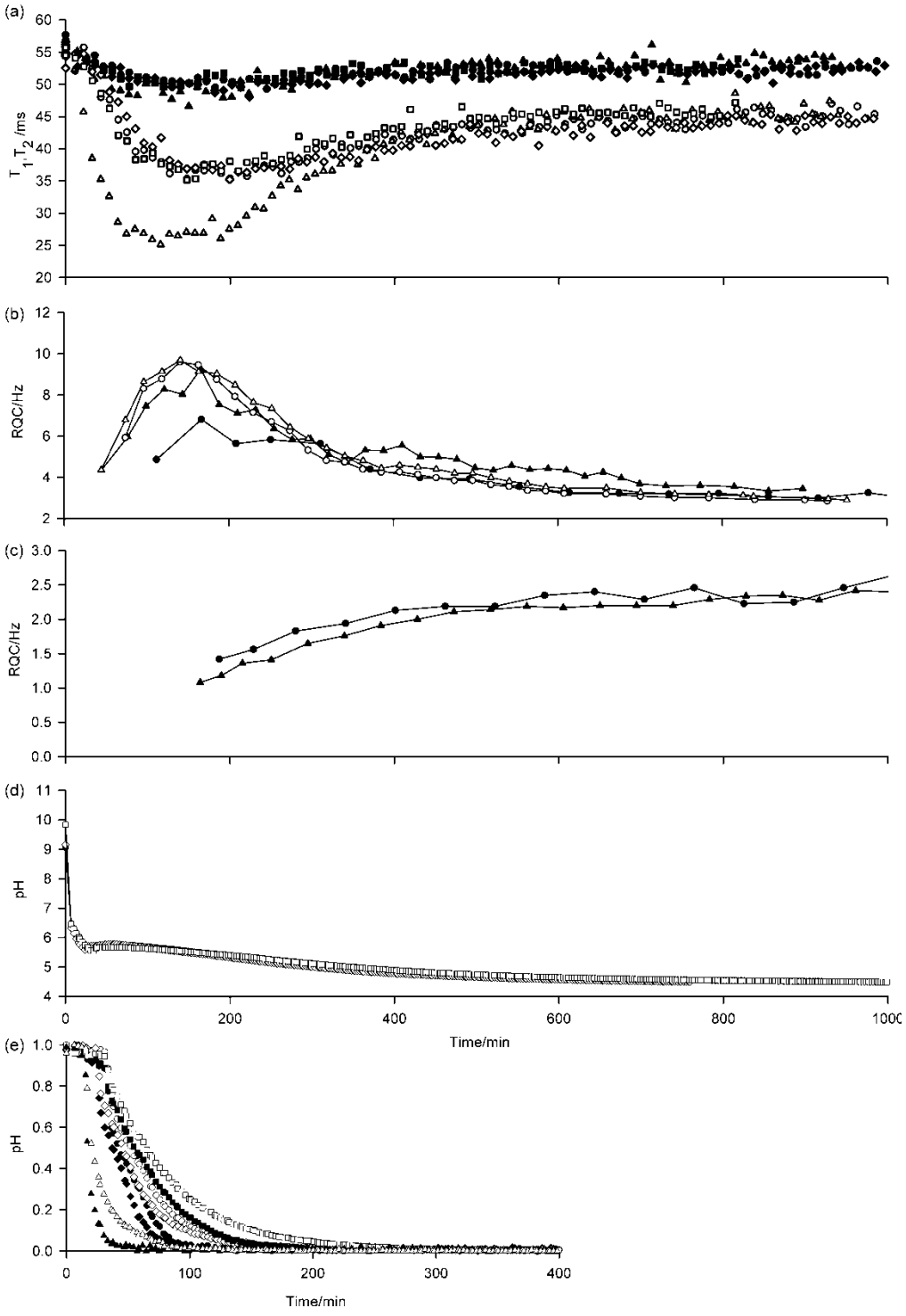

Figure S4a. Plots of experimental parameters versus time during the gelation of **1**. (a) $^{23}Na^+$ T_1 (black) and T_2 (white) relaxation times in the absence of the specified probe molecules from the sample: all probes present (circle), IPA absent (square), NH_4Cl absent (diamond), all probes including pH indicators absent (triangle). (b) $^{14}NH_4^+$ RQCs: all probes present (circle), IPA absent (triangle). The data in white were prepared from the same stock solution of **1** while the data in black were prepared from different stock solutions. (c) IPA RQCs: all probes present (circle), NH_4Cl absent (triangle). (d) ph: all probes present (black diamond), IPA absent (white diamond), NH_4Cl absent (white square). (e) ^1H integrals of **1**, valine methyl (white) and aromatic resonances

(black): all probes present (circle), IPA absent (diamond), NH_4Cl absent (square), all probes including pH indicators absent (triangle).

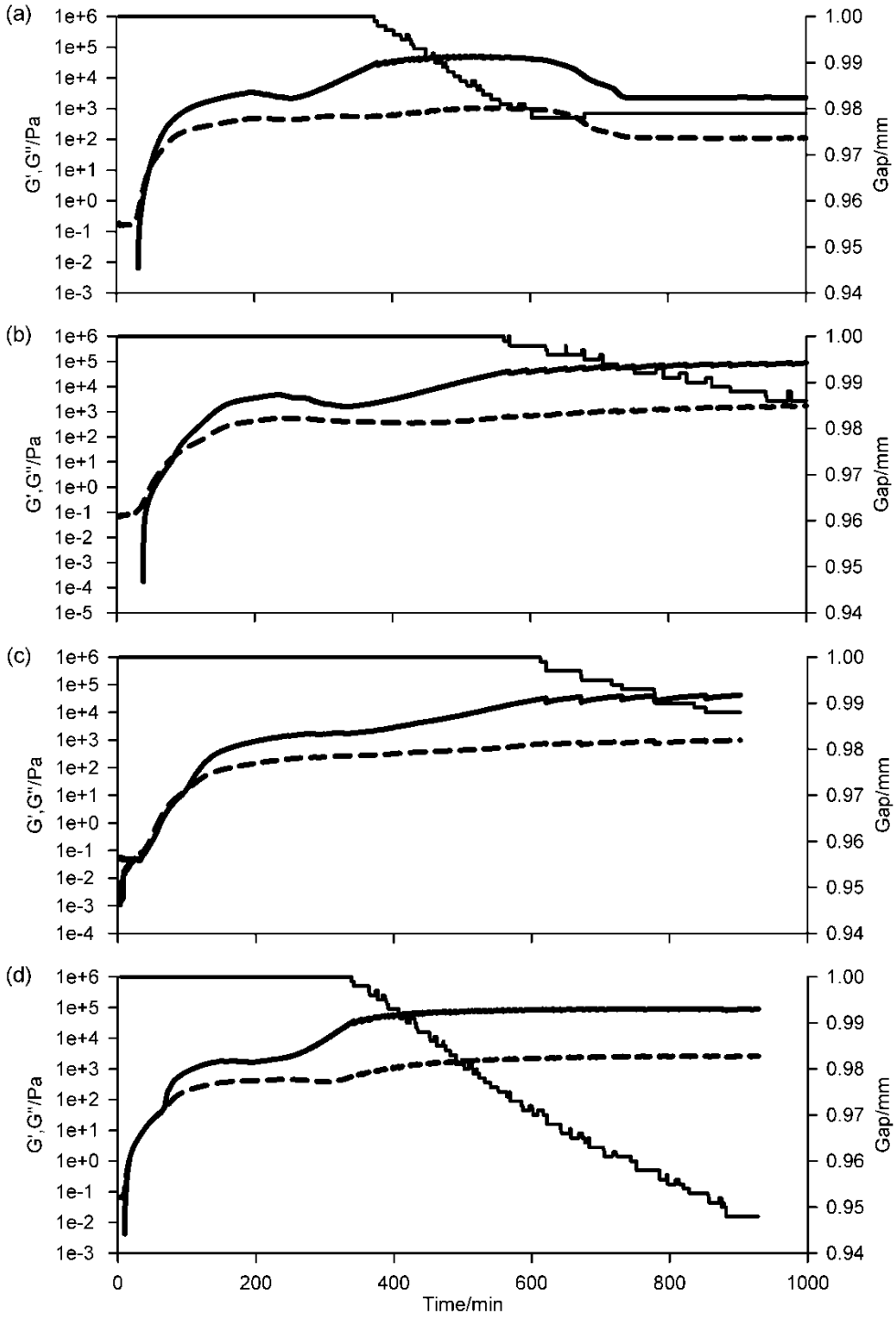

Figure S4b. Plots of G' (thick solid line), G˝ (dashed line) and the gap between the plates of the rheometer (thin line). The specified probe molecules were absent from the sample: (a) All probes present, (b) IPA absent, (c) NH_4Cl absent, (d) IPA, NH_4Cl and pH indicators absent.

The probe molecules for NMR spectroscopy, with the exception of IPA, are not pH neutral and may also affect the hydrolysis kinetics of GdL. The experimental profiles in their presence or absence are thus slightly different, the same quantity of GdL being used for all samples; however, the same general trends as discussed in the main text are apparent. The $^{23}Na^+$ T_2 is markedly reduced in the absence of any probe molecules which is attributable to the much lower total number of positive ions in this sample, each individual Na^+ ion spending a greater fraction of its time associated with the self-assembled fibres relative to the Na^+ ions in other samples. ^1H integrals of **1**, in the absence of any NMR indicators (Figure S4a (d), triangle), were obtained relative to the first spectrum.

5. ^1H NMR spectra of **1** during the early stages of gelation

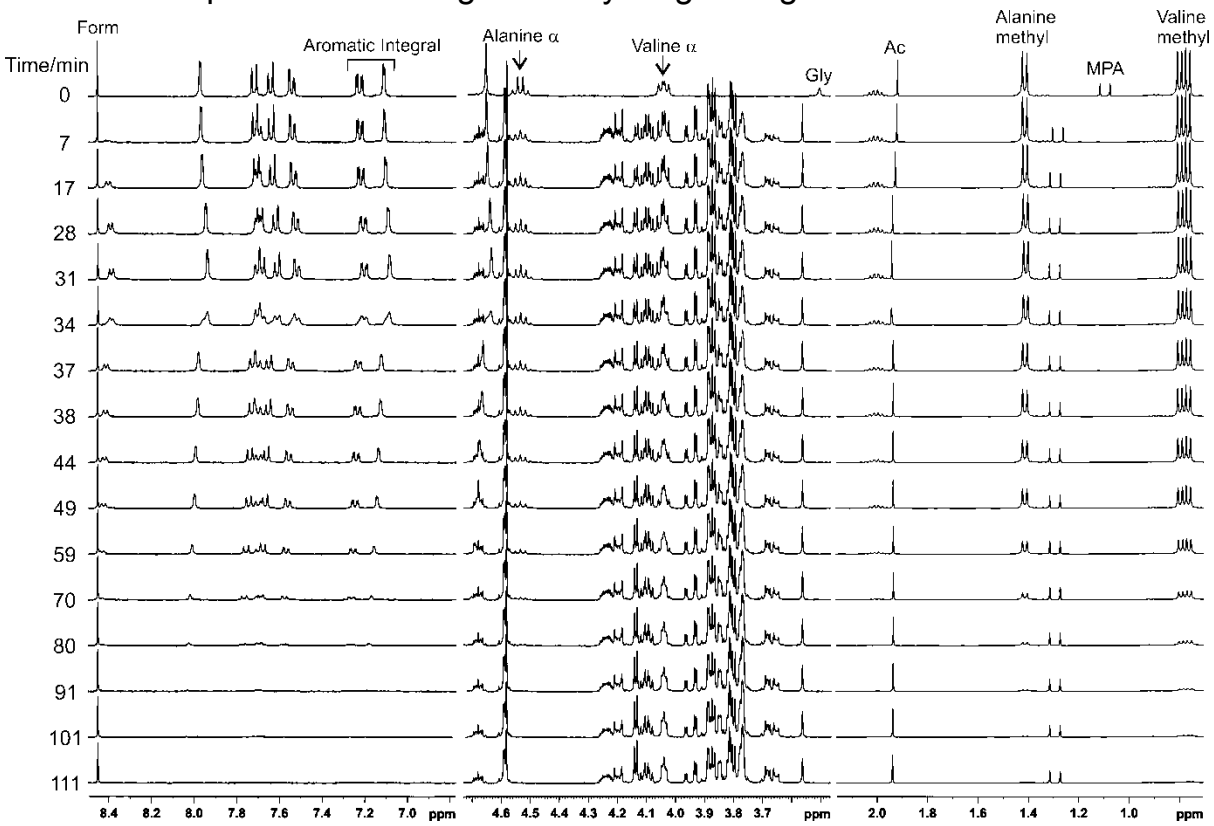

Figure S5. ^1H NMR spectra of sample of Figure 1 (b, c) at times indicated on the left of figure. Resonances of pH indicators are indicated with their abbreviations.

Resonances between 4.7 and 3.6 ppm, unless otherwise indicated, belong to GdL/gluconate. All other resonances belong to **1**. The valine-α resonance overlaps with the H-$C_{(3)}$ resonance of GdL/gluconate at 4.04 ppm;[7] however, the outer peaks of the resonance can be seen to decrease in intensity along with those of the alanine-α proton. The valine-α resonance does not appear to shift significantly between 0 minutes (pH 9) and 60 minutes (pH 5.7) indicating that the NMR-visible gelator is deprotonated. The aromatic resonances indicated by the brackets were integrated over time to obtain the plot on Figure 1b.

6. ^{14}N and ^{2}H spectra of sample of Figure 1a during gelation

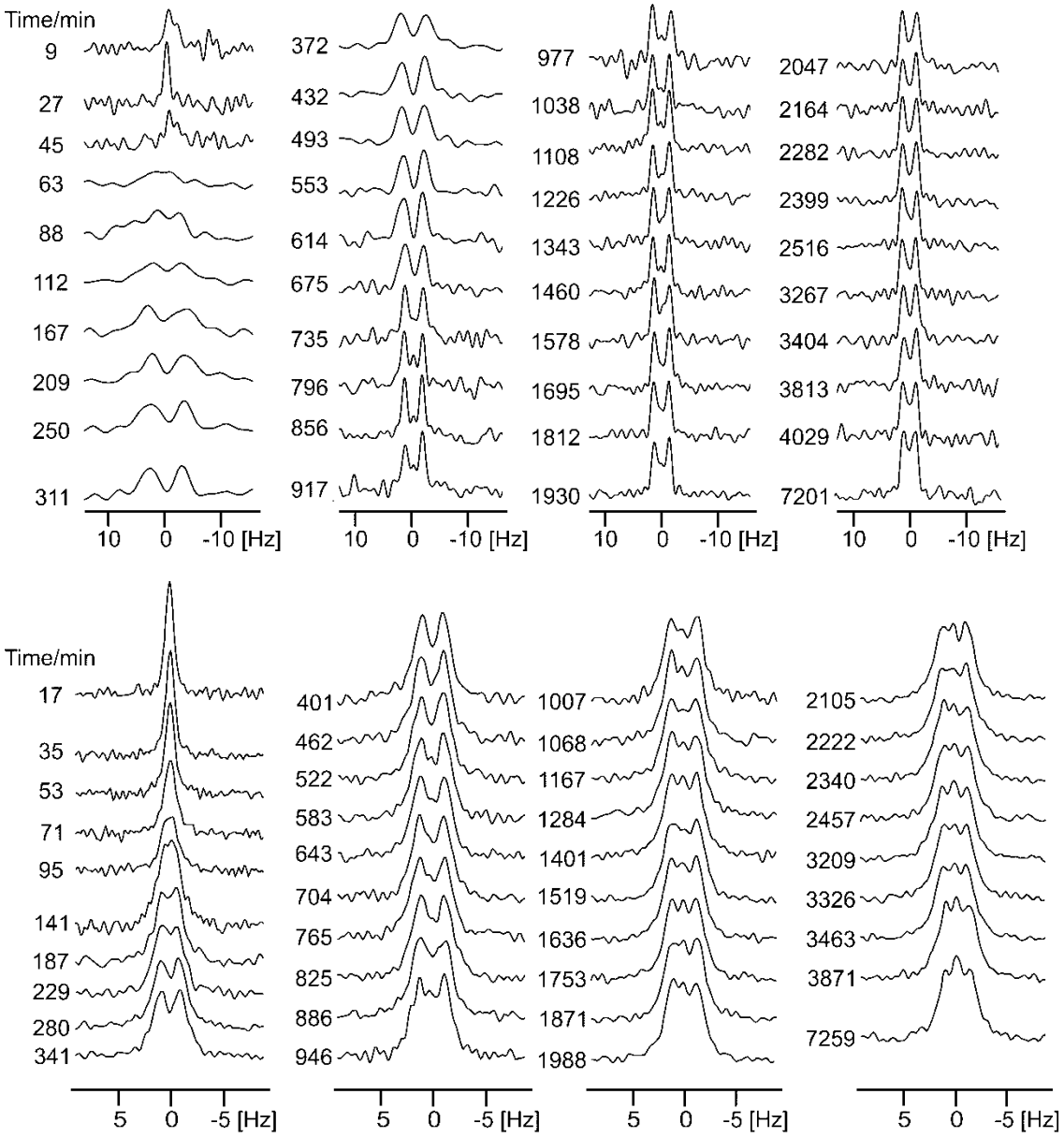

Figure S6a. Experimental ^{14}N (upper plots) and ^{2}H (lower plots) spectra of the sample of Figures 1a and 2 at times indicated since the addition of GdL. The spectra have been scaled to account for the different number of transients recorded at different stages of the gelation process and so the relative intensities of the spectra do not carry any information. The sample was removed from the spectrometer after 4040 minutes and placed in a water bath at 25°C away from the magnetic field. ^{2}H and ^{14}N spectra were recorded again 5 days after the addition of GdL.

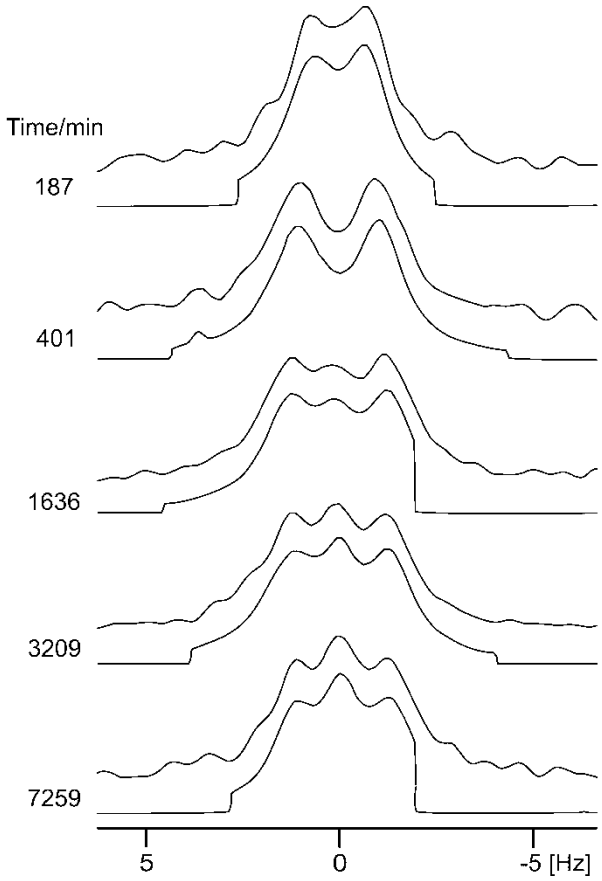

Figure S6b. Selected spectra from Figure S6a, at times indicated since the addition of GdL, to illustrate Lorentzian deconvolution of ^{2}H spectra. Experimental plots are shown above their fits. The RQC was taken as the separation of the outer two Lorentzians forming the doublet. The area of the inner Lorentzian relative to the outer two was taken as the approximate ratio of isotropic solution to anisotropic gel.

7. Profile of ^{23}Na T_1 and T_2 relaxation times in the absence of **1**

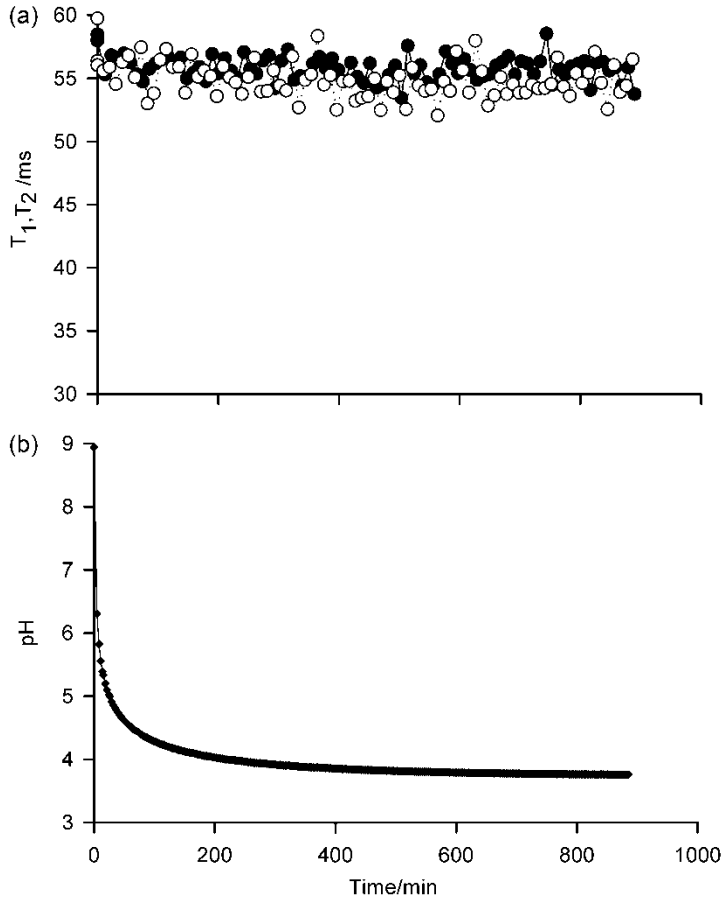

Figure S7. (a) Profiles of $^{23}Na^+$ T_1 (black) and T_2 (white) since addition of 5 mg/mL GdL to a solution of the NMR probe molecules at pH 9 in the absence of **1**. (b) Profile of pH during experiment.

8. NMR analysis of a gel of **1** prepared away from any strong magnetic fields

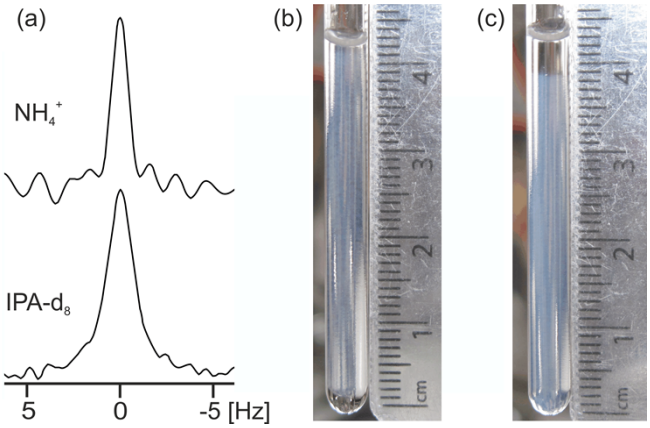

Figure S8. (a) ^{14}N and ^{2}H spectra of a gel prepared away from the magnetic field at 25°C from the same mixture of **1**/GdL as used for the sample of Figures 1a, 2 and S6, analysed 5 days (7200 hours) after the addition of GdL. No residual quadrupolar couplings are detectable, the resonances of IPA and $^{14}NH_4^+$ both being single lines. Macroscopically, this sample (b) had contracted to a similar extent as the sample gelled in the NMR spectrometer (c). In (c) the tube had been knocked slightly causing the gel to slip down to the bottom. ^{23}Na T_1 and T_2 relaxation times in (b) were measured as 53±1 ms and 50±1 ms respectively, compared to 53±1 ms and 48±1 ms in (c).

9. Chemical shift imaging (CSI) analysis of gel of Figure 1a

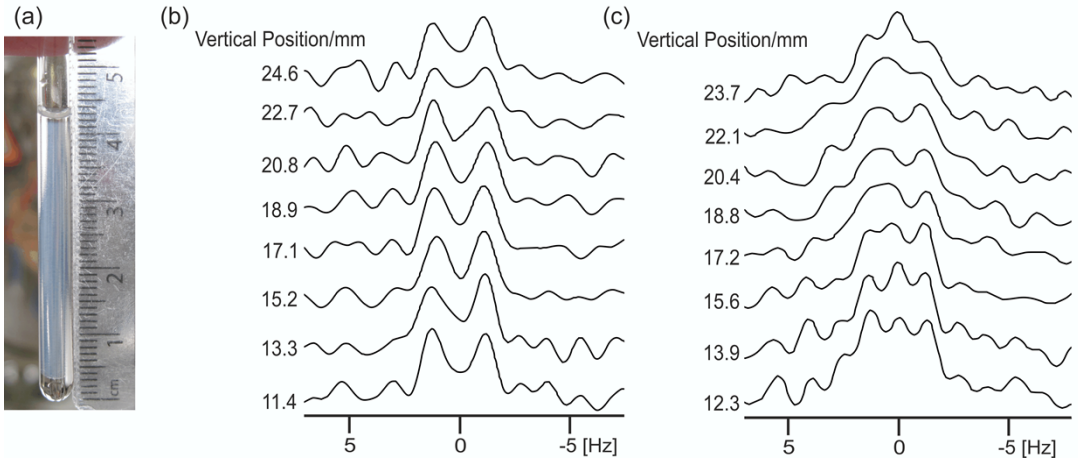

Figure S9. (a) Photograph of gel sample of Figures 1a, 2 and S6, 67 hours after the addition of GdL. (b) ^{14}N spectra (NH_4^+) at indicated vertical position from base of NMR tube (centre of vertical slice), recorded 48 hours after addition of GdL. The $^{14}NH_4^+$ RQC remains homogeneous throughout. (c) ^{2}H spectra (IPA) at indicated vertical position from base of NMR tube, 60 hours after the addition of GdL. The signal to noise ratio of these spectra are poor; however, a doublet and an isotropic peak are discernible at both the lower and upper parts of the NMR active region of the sample.

The ^{14}N chemical shift image was recorded using the sequence of Trigo-Mouriño et al.[5] modified to incorporate the aring ($\pi/2$-τ-$\pi/2$-τ-$\pi/2$) sequence to generate the transverse magnetisation and with CPD (Waltz-16) applied during the pulses and signal acquisition in order to remove the effect of ^{14}N-^{1}H coupling. 16 gradient increments from -52 to 52 G/cm were executed, each with 2048 transients and a gradient pulse duration of 192 μs. 578 data points were acquired with a sweep width of 10 ppm giving a total acquisition time of 11 hours and a theoretical spatial resolution of 1.9 mm. The central time of this acquisition was 48 hours after GdL addition. The ^{2}H chemical shift image was recorded using the sequence: $\pi/2$ - Δ - π - τ_1 - g - τ_2 – acquire, where g is the gradient pulse and Δ = τ_1 + g + τ_2. τ_1 = 10 μs and τ_2 = 200 μs. 16 gradient increments were executed from -52 to 52 G/cm, each with 512 transients and a gradient pulse of 104 μs. 1964 data points were collected with a sweep width of 8 ppm giving a total acquisition time of 5 hours and a theoretical spatial resolution of 1.6 mm.

10. Time-lapse photography and parallel NMR analysis of gelation of **1**

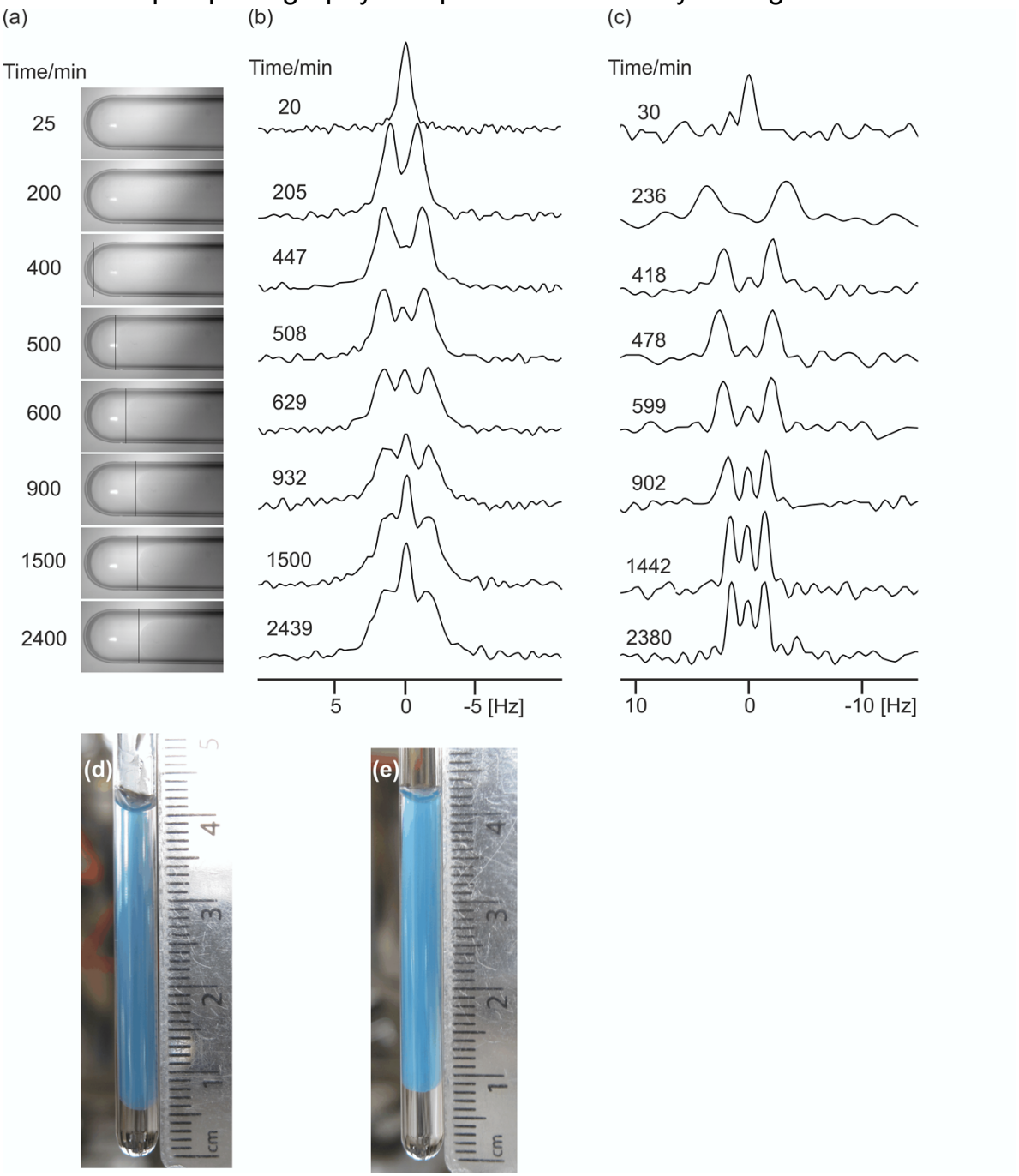

Figure S10. (a) Photographs of NMR tube at times indicated since the addition of GdL. The sample was held in a water bath at 25°C at an angle of ca. 20° to the horizontal. The position of the bottom of the gel is indicated by black lines. Nile blue dye was incorporated to improve contrast, the solution being prepared using the procedure detailed below. (b) ^{2}H (IPA) spectra of a parallel sample at times indicated since the addition of GdL. (c) ^{14}N (NH_4^+) spectra at times indicated since the addition of GdL. (d) Photograph of sample of (a) 68 hours after the addition of GdL showing that the gel has contracted to a similar extent as the sample gelled in the NMR spectrometer (e).

A stock solution of Nile blue dye was prepared by dispersing the solid dye (5 mg) in H_2O (200 mL) and dissolving with repeated stirring and sonication. This solution was used to prepare solutions and gels of **1**, as detailed in the main text.

11. Gelation of **1** with 10 mg/mL GdL

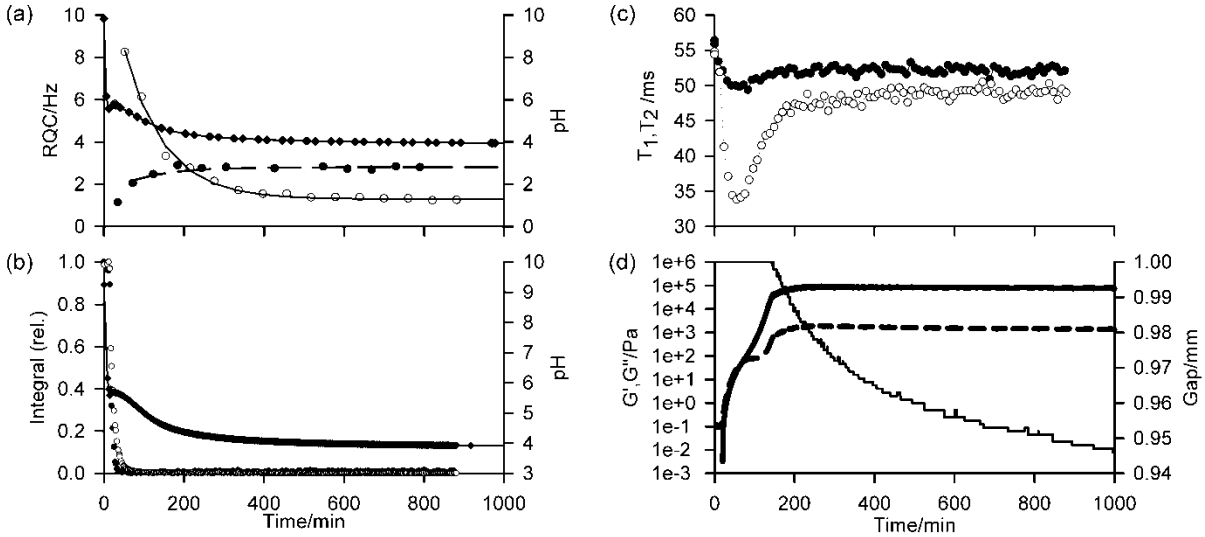

Figure S11a. Time dependent profiles of experimental parameters during gelation of **1** with 10 mg/mL GdL. a) Profile of $^{14}NH_4^+$ (white circle) and IPA (black circle) RQCs. Fits to Equations 4 and 5 are shown with solid and dashed lines respectively. pH is indicated with black diamonds, the solid line is there to guide the eye. Plot of integrals of valine methyl (white circle) and aromatic resonances (black circle) of **1**. pH is indicated with black diamonds. c) Profile of $^{23}Na^+$ T_1 (black circle) and T_2 (white circle). These parameters were recorded on the same sample as (b). d) Profile of G' (thick solid line), G'' (dashed line) and gap between the plates of the rheometer (thin line).

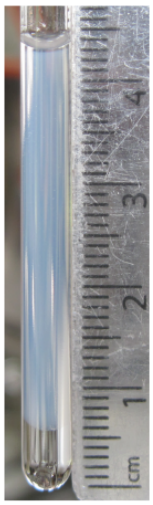

Figure S11b. Photograph of sample of Figure S11a, 20 hours after the addition of GdL.

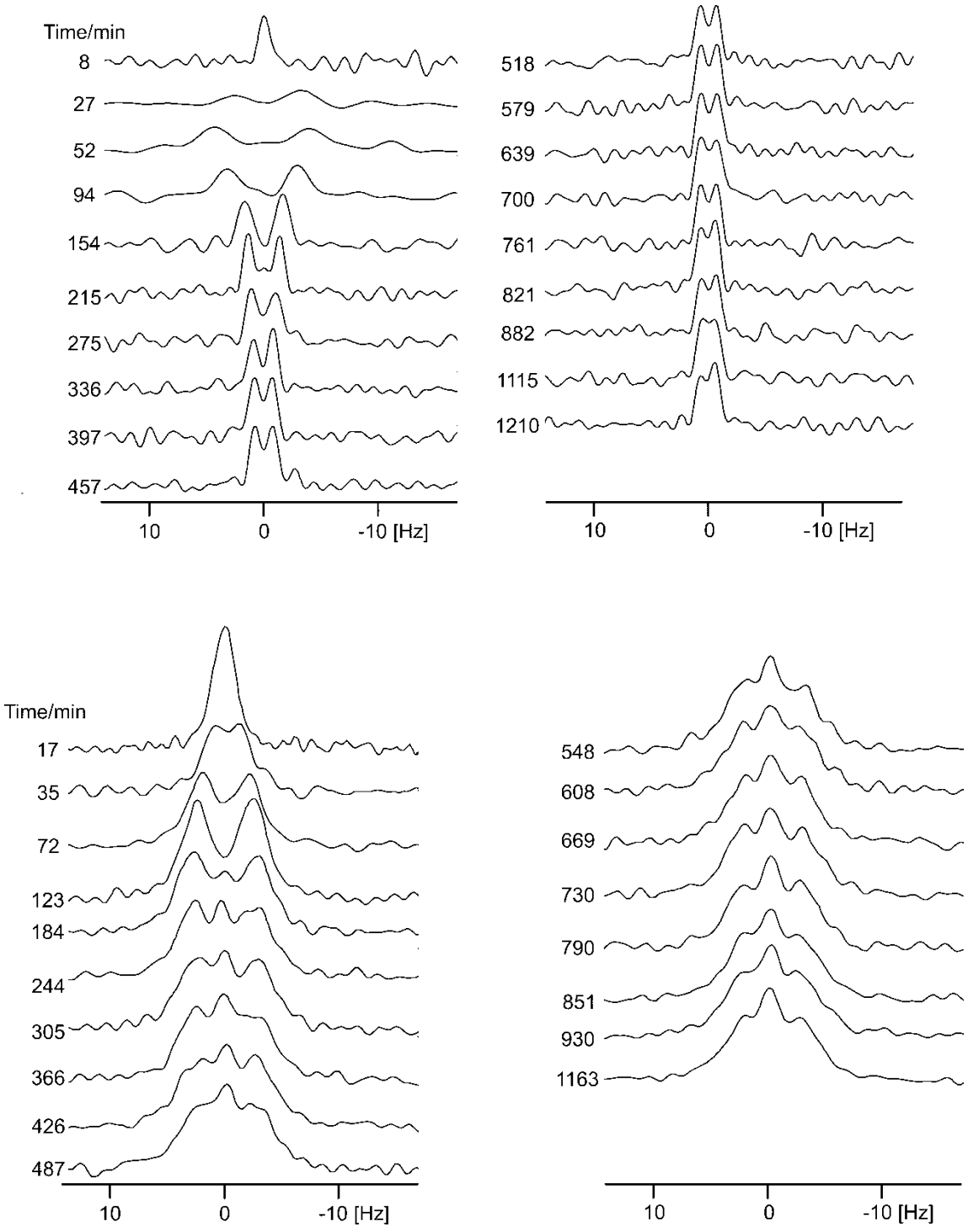

Figure S11c. ^{14}N (upper plots) and ^{2}H (lower plots) spectra at times indicated since the addition of 10 mg/mL GdL to a solution of **1** at high pH.

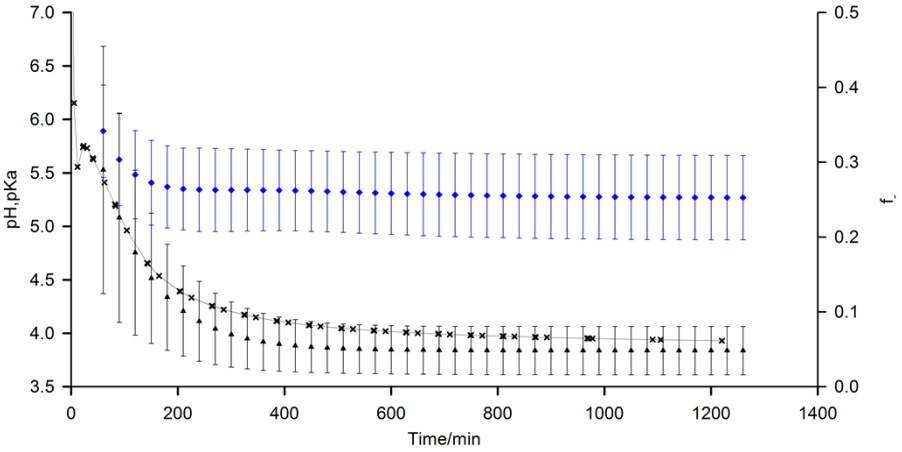

Figure S11d. Plots of f_- (black triangle) and pK_a (blue diamond) values of carboxylate groups on the gel fibres, estimated using Equations 3-5, with error bars calculated using the method described in the ESI, Section 13. pH is indicated with black crosses, the solid line is there to guide the eye.

The experimental parameters follow the same profiles at 10 mg/mL as at 5 mg/mL GdL; however, the sample develops much more quickly. It is possible to estimate the fraction of charged sites, f_-, and pK_a of the carboxylate groups on the gel fibres using Equations 3-5 (Figure S11a, a; Figure S11d). According to our fitting, at 90 minutes since the addition of GdL 20±15% of the carboxylates are deprotonated corresponding to a pK_a of 5.9±0.5 at pH 5.1. At pH 3.9, 5±3% of the carboxylates are deprotonated corresponding to a pK_a of 5.3±0.3. These values are significantly different to those calculated from the 5 mg/mL data; however, the much faster evolution of the system at 10 mg/mL relative to the finite time required to measure a ^{14}N or ^{2}H RQC may have significantly affected the fitting to Equations 4 and 5.

12. Gelation of **1** with 4 mg/mL GdL

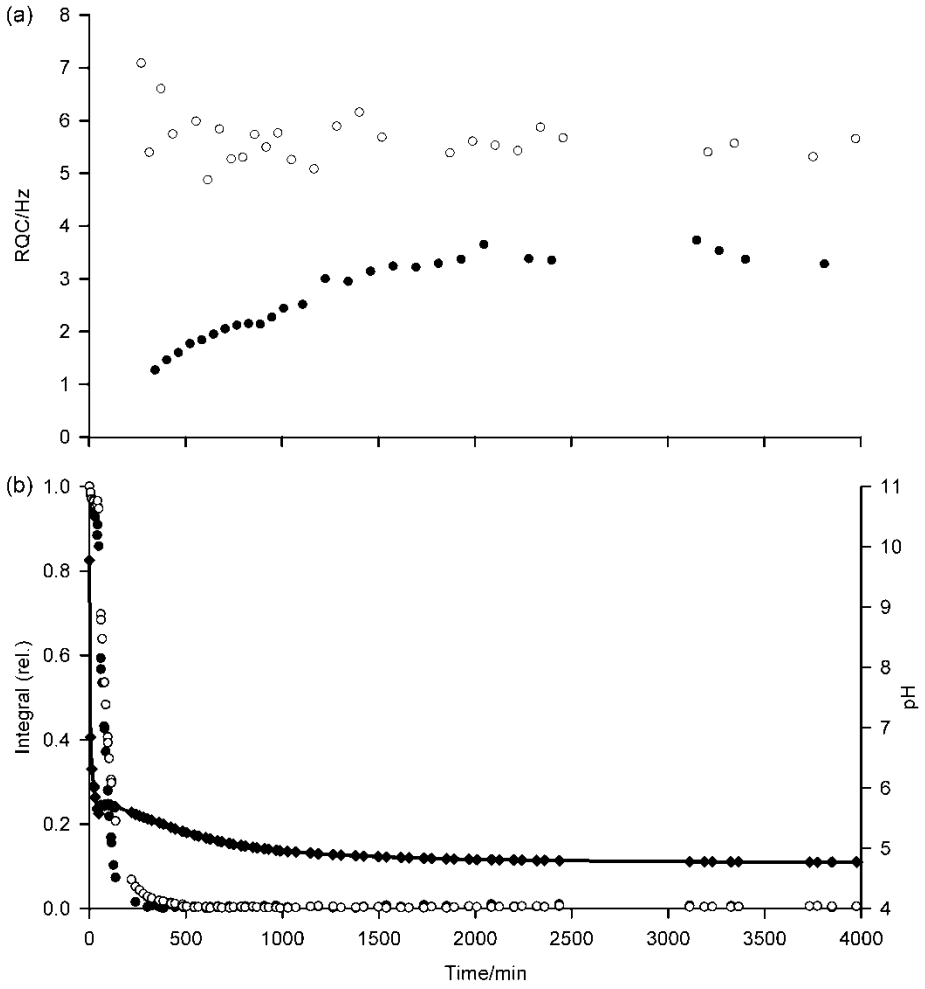

Figure S12a. Time dependent profiles of experimental parameters during gelation of **1** with 4 mg/mL GdL. a) Profile of $^{14}NH_4^+$ (white circle) and IPA (black circle) RQCs. b) Plot of integrals of valine methyl (white circle) and aromatic resonances (black circle) of **1**. pH is indicated with black diamonds, the solid line is there to guide the eye.

Figure S12b. Photograph of gel sample of Figure S13a, 73 hours after the addition of GdL.

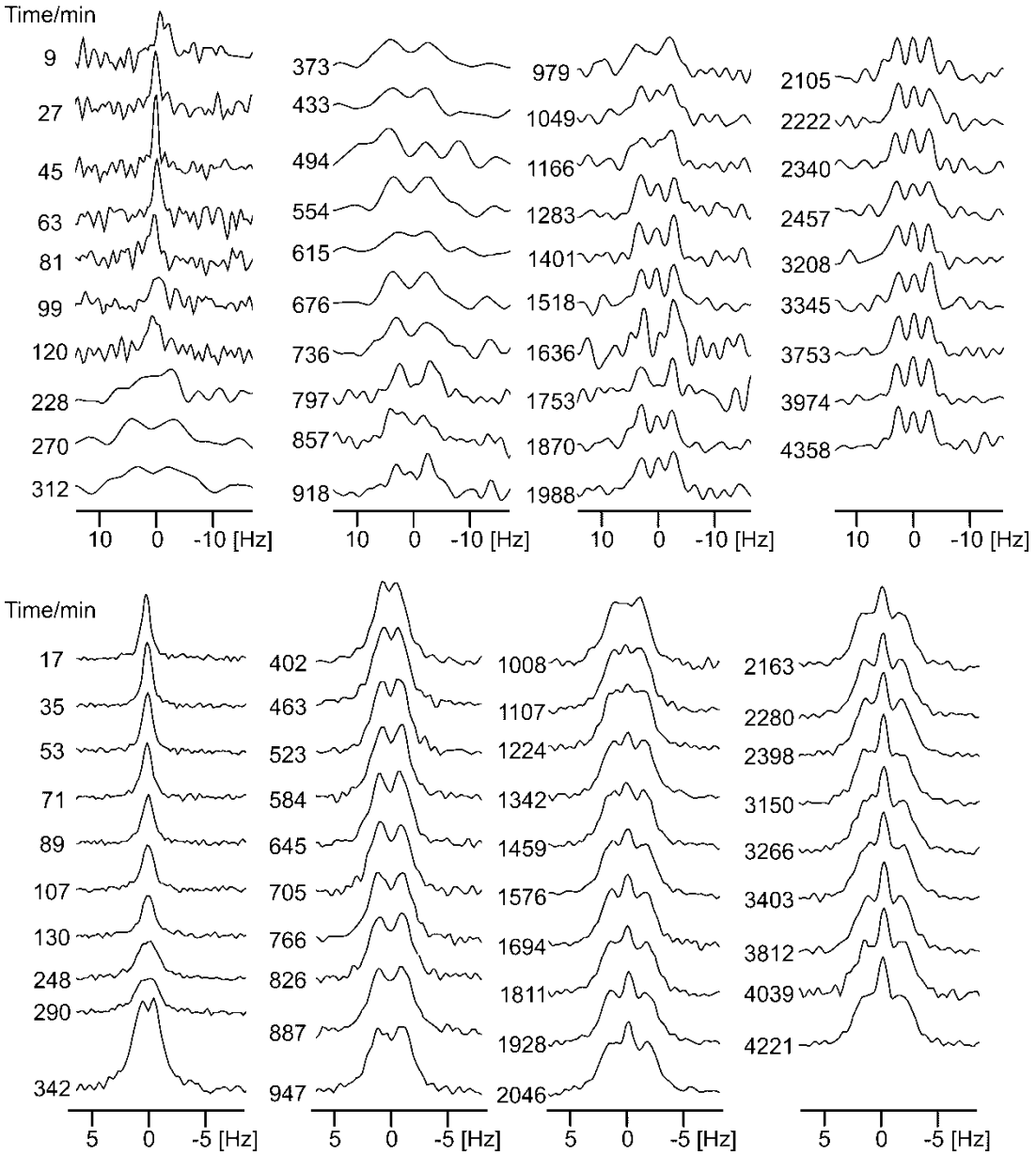

Figure S12c. ^{14}N (upper plots) and ^{2}H (lower plots) spectra at times indicated since the addition of 4 mg/mL GdL to a solution of **1** at high pH.

The gelation kinetics are significantly slower at 4 mg/mL GdL than at 5 mg/mL GdL, the gelator becoming completely NMR invisible only after 500 minutes compared to 200 minutes at 5 mg/mL GdL (Figure 1b). These slower kinetics and significantly higher pH apparently lead to the RQCs of the $^{14}NH_4^+$ and IPA following a different pattern. The charged carboxylate sites on the fibres, which according to our theories (Equations 2 to 5) give rise to the observed RQCs of $^{14}NH_4^+$, may be considered as an intermediate between unassembled gelator and/or pre-fibrillar assemblies that do not contribute to the observed RQCs and protonated carboxylate sites on the gel fibres. The kinetics of assembly and protonation may be such that the $^{14}NH_4^+$ RQC remains almost constant whereas the IPA RQC, which depends on the amount of protonated carboxylate sites on the fibres, increase as these sites are the 'final product' of the assembly process. The integrals of **1** and RQCs of NH_4^+ and IPA at 5 and 10 mg/mL GdL follow a profile resembling that of a sequential reaction that does not go to completion due to the finite amount of GdL added and its weakly acidic nature. The higher charge

of the fibres and slower gelation kinetics with 4 mg/mL GdL may also cause a greater instability of the final gel network resulting in a less homogeneous gel being formed than at 5 and 10 mg/mL GdL, as is apparent by comparing Figure S12b with Figures S11b and 2b; the gels prepared at higher concentrations of GdL, although macroscopically contracted to a similar extent, appear more transparent and homogeneous.

13. Analysis of uncertainty in gel fibre surface charge determination (Equations 3-5) by Monte Carlo simulation

Uncertainties in f_- were estimated using a Monte Carlo method based on that of Lambert et al.[8] Briefly, the standard fitting error of the experimental data to Equations 4 and 5 was used as the standard deviation of sets of randomly generated numbers which were then added to the original fit to generate 50 pseudo-experimental data sets. These datasets were fitted to Equations 4 and 5 to generate 50 sets of fitting parameters. The parameter sets which gave the largest and smallest values of f_- at each time point were then determined with the uncertainty in f_- taken as half of the difference between these values. The uncertainties in the pK_as were similarly computed. The original fitting parameters – those giving the best fit to the experimental data – were used to calculate f_- from Equation 3. The original ^{14}N and ^{2}H experimental data and fits from Figure 3 are shown on Figure S13a below, along with the fits to the pseudo-experimental datasets giving the maximum (red) and minimum (blue) values of f_-. The experimental data was found to be quite reproducible (Figure S13b) with the calculated values of f_- agreeing between the datasets within the estimated uncertainties.

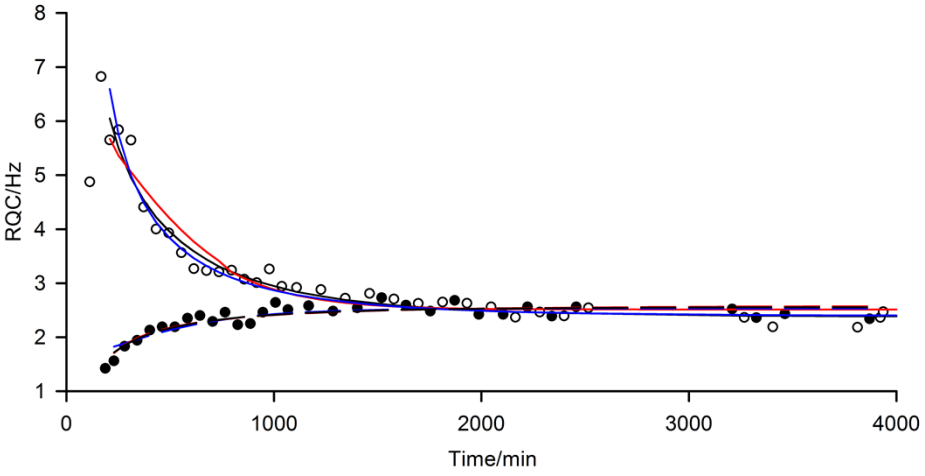

Figure S13a. Plots of $^{14}NH_4^+$ (white circle) and IPA (black circle) RQCs from Figure 4. The fits of Equations 4 and 5 to the experimental data are shown by black solid and dashed lines respectively. The fits of Equations 4 and 5 to the pseudo-experimental datasets giving the largest (red) and smallest (blue) values of f_- are also shown; although not providing as good a fit to the original experimental data, these curves are nevertheless a reasonable representation and so the stated uncertainties in f_- are reasonable estimates.

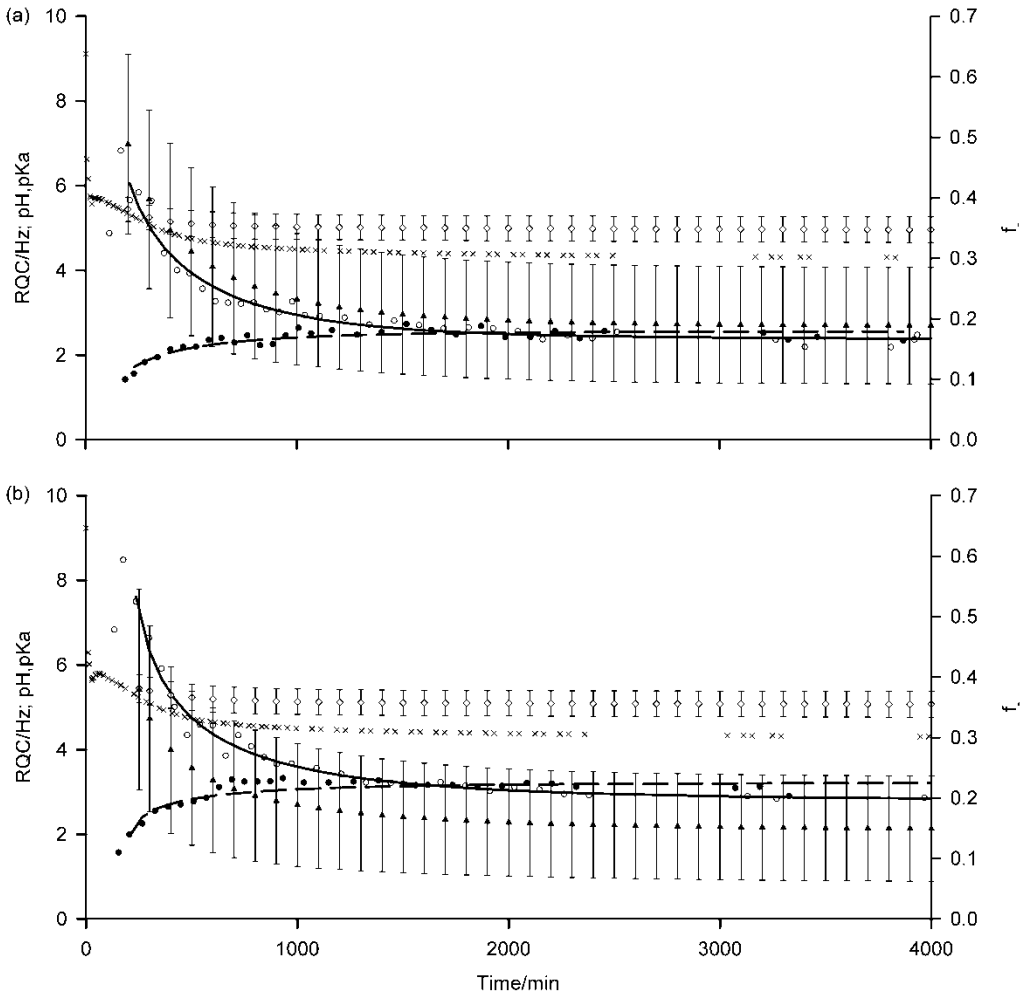

Figure S13b. Plots to show reproducibility of experimental data with gels of **1** prepared with 5 mg/mL GdL; $^{14}NH_4^+$ (white circle) and IPA (black circle) RQCs along with pH data (black cross). Fits of RQC data to Equations 4 and 5 are shown by solid and dashed lines respectively. f_- (black triangle) and pK_a (white diamond) values of carboxylate groups on the gel fibres, estimated using Equations 3-5, are shown with error bars calculated using the method described above. (a) Reproduction of Figure 3 in the main text, provided here for convenience. (b) Replicate of experimental dataset. Estimated f_- and pK_a values of the two datasets agree within the stated uncertainties.

14. Changes to the normal force of the sample during gelation

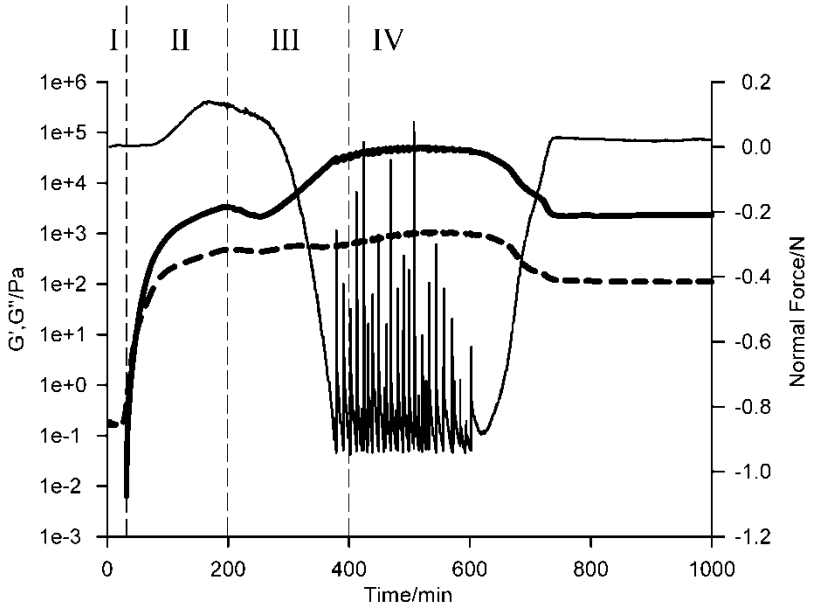

Figure S14. Plot of the normal force (thin line) along with G' (thick solid line) and G'' (dashed line) from Figure 1d. The roman numerals indicate the different phases of the gelation process.

The normal force increases slightly during phase II, concomitant with the formation of a cross-linked network where G' > G'', before decreasing sharply during phase III. Towards the end of phase III, the rheometer decreases the gap between the measurement plates in order to try and increase the normal force back to 0 N (Figure 1d); however, the continued contraction of the sample soon lowers the normal force once more leading to the jagged appearance of the plot. These same trends were apparent in the presence/absence of IPA, NH_4Cl and the pH indicators (data not shown). A decrease in normal force implies a contraction of the sample, as is known to occur during the cross-linking of various polymer systems.[9, 10]

15. Effect of the magnetic field during gelation on the final rheological properties of gels formed from **1.**

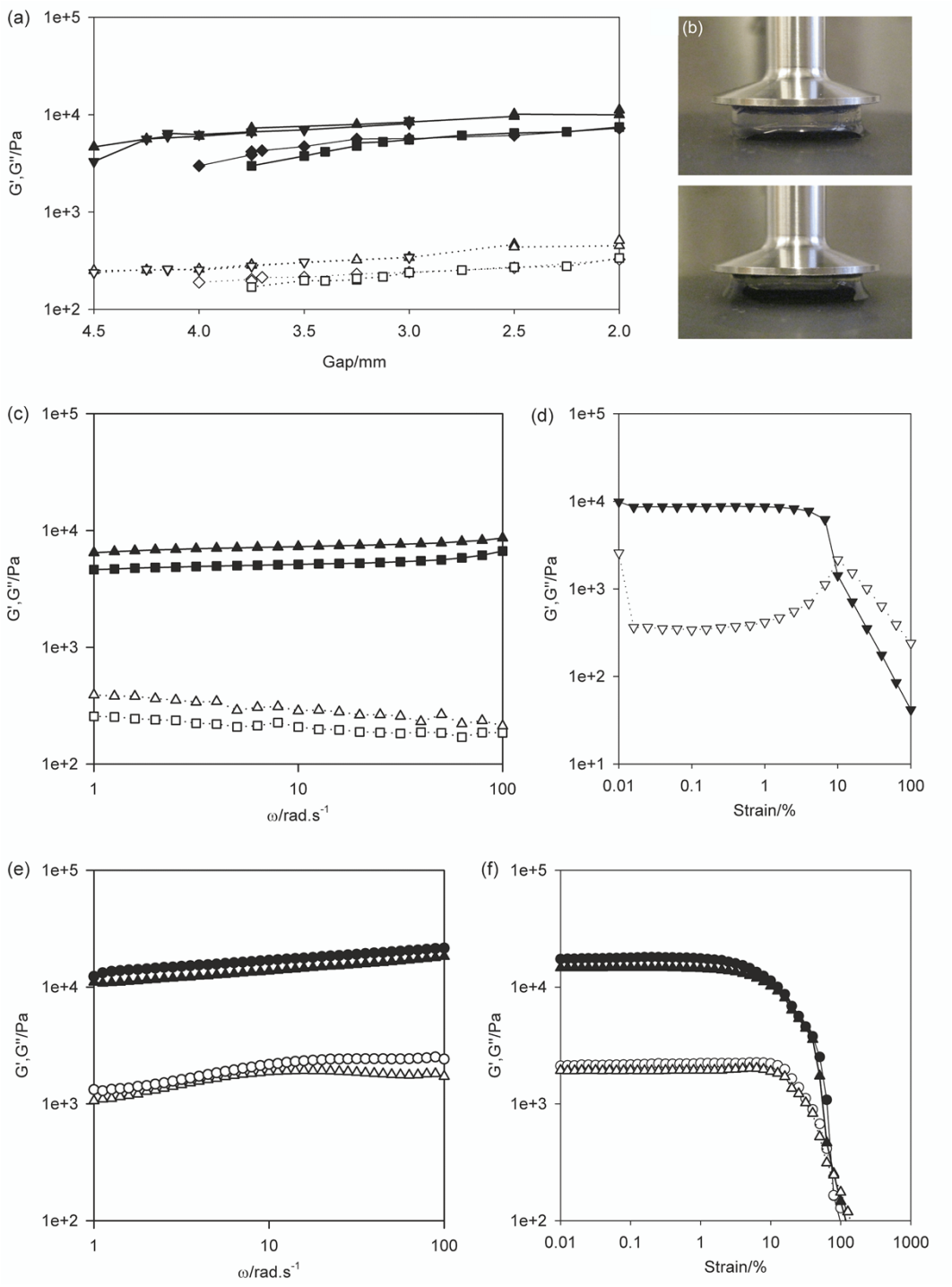

Figure S15. (a) Plots of G' (black) and G'' (white), measured at an angular frequency of 10 rad/s and a strain of 0.1%, versus gap distance for samples prepared in (diamond and square) and away from (up and down triangle) the 9.4 T magnetic field of the NMR spectrometer. (b) Photographs of gel samples during measurements (up triangle, (a)) at 4.5 mm (top) and 3.5 mm (bottom) gaps. (c) Frequency sweeps at 0.1 % strain for samples of (a), the symbols have the same meaning and refer to the same samples as (a). Data for the gel prepared away from the magnetic field (triangle) was recorded at a gap of 3.75 mm and data for the

sample prepared in the field (square) was recorded at a gap of 3.25 mm. (d) Strain sweep, recorded at an angular frequency of 10 rad/s, of a gel prepared away from the magnetic field (down triangle, (a)) at a gap of 3 mm. (e) Plots of G' (black) and G'' (white) versus frequency, recorded at a strain of 0.1%, of gels prepared in (triangle) and away from (circle) the magnetic field of the NMR spectrometer in 4 mL Sterilin polystyrene vials. (f) Strain sweeps, recorded at an angular frequency of 10 rad/s, for the samples of (e).

The gels samples of Figures S15a-d were prepared in 20 mL polypropylene syringes. The barrels were sawn down to provide a tube while the plungers had been sawn so that the syringes could be stood on their flanges and easily lowered into the NMR magnet (9.4 T) in a cradle. To analyse the gels, the plungers were gently pushed up out of the barrels and the gels slid onto glass slides before being transferred to the lower (silicon rubber) plate of the rheometer (Anton Paar Physica MCR101). The upper plate (25 mm, sandblasted) was then lowered while the gel was centred by eye. Once the plate was just in contact with the sample, a frequency sweep was recorded between 5 and 20 rad/s at 0.1% strain. The upper plate was then lowered and the frequency sweep repeated to produce the plots of Figure S15a. At a gap of 2 mm, all gels were excessively squashed with very significant volumes of water exuded and so the rheological measurements most representative of the bulk gels are those recorded at intermediate gaps (Figure S15c). From Figures S15a-d, it is apparent that the gels prepared in the magnetic field of the spectrometer are slightly weaker than those prepared away from the field; however, they have broadly similar mechanical properties. Similar data was obtained when the gels were prepared in 4 mL Sterilin polystyrene sample vials and analysed with a vane and cup geometry (Figures S15e-f). The vials had been roughened with sandpaper prior to use and served as the holder for the gels during the measurements. Inspection of the gels after the strain sweeps revealed that the gels had fractured internally rather than at the walls of the vial. All the samples of Figure S15 were prepared using the same mixture of **1** with GdL at ambient temperature (20-21 ^{o}C), with the other additives used for the NMR experiments also included. The development of a gel at this ambient temperature was found by NMR to be very similar to the development at 25^{o}C (data not shown), with very similar magnetic-field-induced anisotropy apparent. All rheological measurements were performed at 25^{o}C. The samples were analysed between 16 and 19 hours after preparation.

References

1. A. M. Brown, *Comput. Methods Programs Biomed.*, 2001, **65**, 191-200.
2. Z. Szakács, G. Hägele and R. Tyka, *Anal. Chim. Acta*, 2004, **522**, 247-258.
3. W. M. Haynes, ed., *CRC Handbook of Chemistry and Physics*, 95th edn., CRC Press, Boca Raton, FL, 2014.
4. P. C. Crofts and G. M. Kosolapoff, *J. Am. Chem. Soc.*, 1953, **75**, 3379-3383.
5. P. Trigo-Mouriño, C. Merle, M. R. M. Koos, B. Luy and R. R. Gil, *Chem. Eur. J.*, 2013, **19**, 7013-7019.
6. M. Liu, X. A. Mao, C. Ye, H. Huang, J. K. Nicholson and J. C. Lindon, *J. Magn. Reson.*, 1998, **132**, 125-129.
7. A. Pallagi, P. Sebk, P. Forgó, T. Jakusch, I. Pálinkó and P. Sipos, *Carbohydr. Res.*, 2010, **345**, 1856-1864.
8. R. J. W. Lambert, I. Mytilinaios, L. Maitland and A. M. Brown, *Comput. Methods Programs Biomed.*, 2012, **107**, 155-163.
9. L. Matějka, *Polym. Bull.*, 1991, **26**, 109-116.
10. M. Harsch, F. Herzog and J. Karger-Kocsis, *J. Compos. Mater.*, 2008, **42**, 2299-2309.